Design Improvements and System Identification of PARTNER, a Rehabilitation Robot

A Thesis

Presented in Partial Fulfilment of the Requirements for the

Degree of Master of Science

with a

Major in Mechanical Engineering

in the

College of Graduate Studies

University of Idaho

by

Stephen A. Goodwin

Major Professor: Eric T. Wolbrecht, Ph.D.

Committee Members: Joel C. Perry, Ph.D.; Michael J. Anderson, Ph.D.

Department Administrator: Steven W. Beyerlein, Ph.D.

August 2017

Authorization to Submit Thesis

This thesis of Stephen A. Goodwin, submitted for the degree of Master of Science with a major in Mechanical Engineering and titled "Design Improvements and System Identification of PARTNER, a Rehabilitation Robot," has been reviewed in final form. Permission, as indicated by the signatures and dates below, is now granted to submit final copies to the College of Graduate Studies for approval.

Major Professor:	_____ Eric T. Wolbrecht, Ph.D.	Date:	_____
Committee Members:	_____ Joel C. Perry, Ph.D.	Date:	_____
	_____ Michael J. Anderson, Ph.D.	Date:	_____
Department Administrator:	_____ Steven W. Beyerlein, Ph.D.	Date:	_____

Abstract

Stroke rehabilitation is a rapidly growing research field in the engineering community. The introduction of robotics into traditional rehabilitation regimes brings exciting potential benefits including lower costs, increased dosage, increased motivation, and improved quantification of the rehabilitation process. This thesis presents mechanical design improvements of PARTNER, the Parallel Actuated Robotic Trainer for NEuroRehabilitation, a robot designed to provide spatial assistance during robotic therapy while exhibiting low-impedance, high backdrivability, and spatial uniformity characteristics. Specific mechanical designs of the robot's structure, bearing assemblies, and linkages are described in detail. Additionally, some safety features and control system pieces are discussed. Finally, frequency response data of the system is presented alongside a fitted second-order dynamic model.

Acknowledgements

First and foremost, I thank my major professor, Dr. Eric Wolbrecht for all the expertise, assistance, and patience during my graduate studies. His excitement for research and academics enriched my time at the University of Idaho greatly. I thank Dr. Joel Perry and Dr. Michael Anderson for serving on my committee and providing valuable insights during the writing and defending processes. Additionally, I thank Dr. Steven Beyerlein for the many years of encouragement, service, and mentorship through my entire University of Idaho career.

I'd like to thank friends and fellow students for the enormous support gifted to me throughout all my education. From the countless late homework nights, weekend machine shop days, and test study sessions, to the grad student lunches, coffee breaks, and "training projects", you truly made it a joy to be a student at the University of Idaho.

Research and development on the PARTNER robot has been conducted by a team of talented faculty and students. Of note are student contributions of Hossein Taheri, James Tigue, and Kevin Witkoe. Additionally, machine shop manager Russ Porter is acknowledged for his mentorship and support in fabrication endeavors.

This research was supported by NIH-R01HD062744 from the National Center for Medical Rehabilitation Research at the National Institute of Child Health and Human Development, and the National Center for Research Resources and the National Center for Advancing Translational Sciences, National Institutes of Health, through Grant UL1 TR000153. The content is solely the responsibility of the authors and does not necessarily represent the official views of the NIH.

Thanks are also given to the Idaho Space Grant Consortium for financial support through the Robotic Lunar Exploration Program and Graduate Research Fellowships.

Dedication

This thesis is dedicated to my father, Marc Steven Goodwin,

who spent his life educating, loving, and inspiring.

Table of Contents

List of Tables

List of Figures

Chapter 1: Introduction

1.1 Stroke Rehabilitation

Stroke is a leading cause of disability, with the number of annual incidents near 800,000 in the US [1] and 16.9 Million worldwide [2]. Of survivors, nearly two thirds have reported non-use or disuse of the affected limb at four years post incident [3]. Despite the severity of impairment, only 24% of patients are discharged into an inpatient rehabilitation facility; a further 31% of patients are discharged into outpatient rehabilitation. The reason for relatively low rehabilitation enrollment is largely due to cost [4]. Indeed, the effect of stroke extends beyond personal recovery efforts, with the annual economic load on the US healthcare system estimated to be $71.6 billion. Furthermore, it's expected to triple to $184.1 billion in the next 14 years [1]. Both the human and economic consequences of stroke are humbling and make it clear that research into treatment and care is warranted.

Conventionally, stroke rehabilitation consists of intensive physical therapy with an emphasis on starting the therapy regimen as soon as possible [5]. Exercises such as reaching, grasping, and object manipulation are common when upper-limb impairment is present. These exercises are often performed one patient at a time with some combination of the following trained personnel present: physical therapist, physical therapist assistant, physical therapy aides, and students. A study of approximately twenty-two thousand therapy sessions showed that 64% of sessions are attended by a physical therapist and that only 10% of sessions consist of more than one patient being treated by a single provider [6]. This model of rehabilitation, while effective in getting quality therapy to the patient, is very cost prohibitive and often leads to less therapy per patient than necessary.

The research community has some consensus on best practices in stroke recovery. First, it is generally accepted that motor learning gains are highly coupled with dose of rehabilitation, with more time spent in rehabilitation leading to more motor recovery [5, 7-12]. It is also accepted that passive movement therapy is insufficient; active patient engagement during therapy is necessary [13, 14] to promote neurorehabilitation. Researchers and clinicians are also in general agreement that functional, or task-oriented training is superior to analytical methods of rehabilitation [15, 16]. Analytical methods refer to training individual components of movement, such as elbow flexion/extension or wrist pronosupination. The theory is that by training individual components of tasks, the patient can combine these base movements into a variety of functional tasks. Alternatively, task-oriented therapy focuses on retraining real-world tasks, or activities of daily living (ADLs) directly [17]. They usually consist of multi-joint movements or movements with clear functional goals.

Recently, there has been an emergence of robotic tools designed for use in neurorehabilitation. The potential benefits of robotic devices in post-stroke therapy are numerous and promising [18]. They may enable therapy providers to administer exercises to multiple patients simultaneously, reducing healthcare costs in the long-term. They also are commonly coupled with intuitive video-type games, which can lead to increased patient engagement and therapy dosage, both of which have been identified as key factors in recovery [19]. Other identified benefits include improved matching of patient impairment and applied assistance [15] and the quantification of therapy including patient characteristics, dosage, content, and clinical outcomes [18, 20].

The clinical efficacy of rehabilitation robotics is still being investigated, with a need for increased randomized clinical trials (RCTs) directly investigating the functional outcomes of

robot-aided therapy. So far, systematic reviews have found that robot-aided therapy is capable of matching, and in some cases surpassing, motor-control improvements with respect to conventional therapy [21-23]. Some RCTs have shown that intensive robot-assisted rehabilitation can improve moderate to severe upper limb impairment more than intensive traditional therapy in both acute stroke patients [24] and in chronic stroke patients [25]. These early promising results along with the variety of potential benefits robotic devices possess are a clear indication that robotics in the rehabilitation environment will continue to grow and hopefully improve the lives of many stroke survivors.

1.2 Previous Upper-Limb Rehabilitation Robots

Devices developed for use in upper limb rehabilitation generally are categorized based on the interface between the device and the patient. Exoskeletons robots, such as CADEN-7 [26], Harmony [27], and the ARMin [28] (commercialized as the ArmeoPower), are designed to anatomically mimic the patient's limbs and joints with robot links, connected at multiple positions along the arm. This enables the robot, and subsequently the therapists, clinicians, and researchers, to provide assistive torques at specified joints. This is a huge benefit, enabling more control of the patient during therapy. However, the serial-chain nature of exoskeletons generally leads to large, heavy components. This stems from proximal (shoulder side) components carrying the loads from all distal (hand side) components. This added weight often leads to high mechanical impedance, an undesirable trait in rehabilitation robotics [29]. The effect of this can be minimized through careful mechanical designs [26] and control system implementations [29], but at the cost of added complexity.

The other category of upper limb devices are end-point or end-effector robots. Rather than following the arm from the shoulder down and connecting at multiple locations, end-effector

robots are attached to the user only at a single location. Because of this, the robot loses the ability to assist specific joints in movement, but it does retain the ability to aide in task-oriented training. Benefits of end-effector robots include the option to place the device anywhere with respect to the user, the relative simplicity of mechanical designs, and the relative simplicity of end-point control.

One of the first and most researched devices in rehabilitation robotics is the MIT-Manus [30]. It is a 2-DOF planar end-effector robot that sits on tabletop and placed in front of the patient. The robot is an excellent example of how parallel topologies can be used to increase backdrivability without sacrificing force output. Due to the initial success, it has continued to be a platform of research both in mechanism and clinical domains. Modules have been developed to aid in wrist and hand rehabilitation [31], as well as a vertical spatial extension to provide full translational motion [32].

Another end-effector robot is the 5 DOF device, ACRE [33]. It is grounded to the side and slightly behind the user and connected to his/her forearm. It is a serial-chain topology, but the links are not intended to mimic the anatomy of the upper-limb. The device has an adjustable gravity compensation mechanism that provides a good example of mechanical design choices that reduce the torque requirements for actuators, thus reducing the mechanism size and inertia. However, the designers noted that the dynamics introduced by this mechanism led to unwanted movements and posed a safety hazard.

There are a variety of other end-effector robots that attempt to solve current problems in rehabilitation robots. The Maribot [34] is a wire-based end-effector that is designed to be intrinsically safe and out of the patients way. CRAMER is a forearm and wrist rehabilitation device that was developed with the goal of creating a truly low-cost device by utilizing off-

the-shelf components and a commercially-available gaming platform [20]. There have been multiple literature reviews conducted to survey devices targeted at neurorehabilitation that provide a complete overview of common characteristics and lists of published devices. For further information please see [35-37].

1.3 PARTNER Background

In an effort to push the knowledge base and state of the art in rehabilitation robotics, faculty and students at the University of Idaho have developed PARTNER: the Parallel Actuated Robotic Trainer for NEuroRehabilitation. PARTNER is a 4-degree-of-freedom (DOF) end-effector robot designed to aid in upper-limb rehabilitation of neurological disorders, principally post-stroke effects. The robot's defining characteristics are an inherent low mechanical impedance and a high backdrivability that is consistent across all three translational degrees-of-freedom. Both of these characteristics are desirable in rehabilitation robotics for two main reasons. First, they both are directly related to safety with human patients [30]. Powerful, stiff robots possess the ability to force the upper limb into unnatural positions, causing harm to users. Secondly, these characteristics maintain a causal relationship between the arm and the robot, which is thought to encourage motor-learning by allowing movement errors and correction during therapy [38-40].

The robot, pictured below in Figure 1.1, is based on a modified DELTA topology presented in [41], in which four R-U-U kinematic chains emanate from a common base to a common end-effector in parallel. This topology places all actuated joints, the four parallel revolute joints, on the common base removing their mass from the translating end-effector. Additionally, the removal of actuator weight from distal links on the robot leads to reduced stresses in the members, and thus smaller, lighter links. The actuators (Dunkermoteren STA-

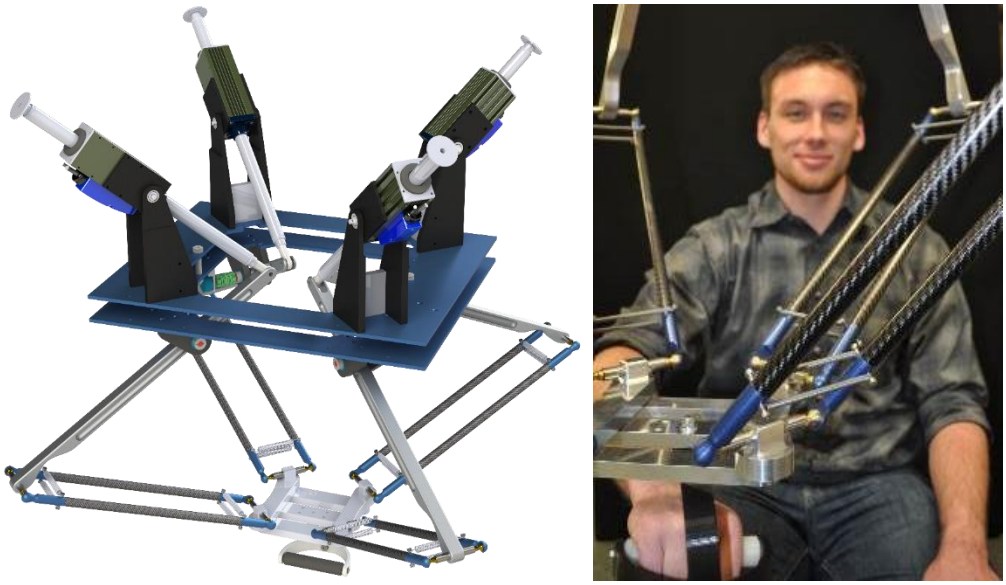

Figure 1.1 The PARTNER robot. A 3D CAD model of the device is shown on the left and a user interacting the device is shown on the right.

2504) are low-friction gearless drives oriented such that the heavy actuator rods counterbalance the mass of the robot links. The chosen robot topology and cascading design implications are the main driving force behind the low mechanical impedance and high backdrivability characteristics of PARTNER.

PARTNER was first developed by Dr. Hossein Taheri as a portion of his Ph.D. dissertation in collaboration with his major professor, Dr. Eric Wolbrecht, and fellow students at the University of Idaho: James Tigue, Kevin Witkoe, and the author of this thesis, Stephen Goodwin. Additional information regarding the design and development of PARTNER can be found in [42, 43].

1.4 Thesis Overview

The remaining chapters in the thesis present work performed in the development of the PARTNER robot and associated efforts. Chapter 2 describes mechanical revisions to PARTNER, including a revised frame, bearing assemblies, improved parallelogram mechanism, and redesigned end-effector rotation mechanism. This is followed in Chapter 3

with details regarding the control electronics, safety system, gravity compensation model, and frequency response data from PARTNER. Chapter 4 concludes this thesis with a final summary of works completed and suggestions for future work on the PARTNER system.

Portions of this thesis have been accepted and published in the proceedings of the 38th International Conference of the IEEE Engineering in Medicine and Biology Society (EMBC 2016) under the title "Design and Optimization of PARTNER: a Parallel Actuated Robotic Trainer for NEuroRehabilitation" [43].

Chapter 2: Mechanical Design

As mentioned in Section 1.3 , initial development of the PARTNER robot began as a portion of Dr. Hossein Taheri's doctoral dissertation [42]. It was in this stage that high level design decisions such as mechanism, actuator, and control electronics selections took place. From a mechanical standpoint, an initial functional alpha-prototype was designed and constructed. This device was able to show that the robot design was valid and worthy of further investigation. However, the device did contain a multitude of design flaws that were discovered in initial testing.

This chapter provides details on multiple mechanical design features of PARTNER. Section 2.1 provides a general overview of the mechanical design of the robot. In Section 2.2 the structure of the robot is discussed with subsections dedicated to the frame and mounting plates. Section 2.3 discusses the design of the pivot bearing assembly. Section 2.4 describes the design of the parallelogram mechanism that is key to the kinematics of the robot. Finally, Section 2.5 discusses the design of the end effector rotation mechanism.

2.1 General Mechanical Design

The PARTNER robot consists of four independently actuated arms that run in parallel from a common base to a common end-effector as shown in Figure 2.1. Each parallel arm can be viewed as two coupled kinematic chains. The first starts with the linear actuators (Dunkermoteren STA 2504) mounted on a pivot bearing located at Point A on the right side of Figure 2.1. The actuators are then connected to Link 2 via a revolute joint. This link is rigidly mounted to the common base on the bottom of the frame via another revolute joint, closing the

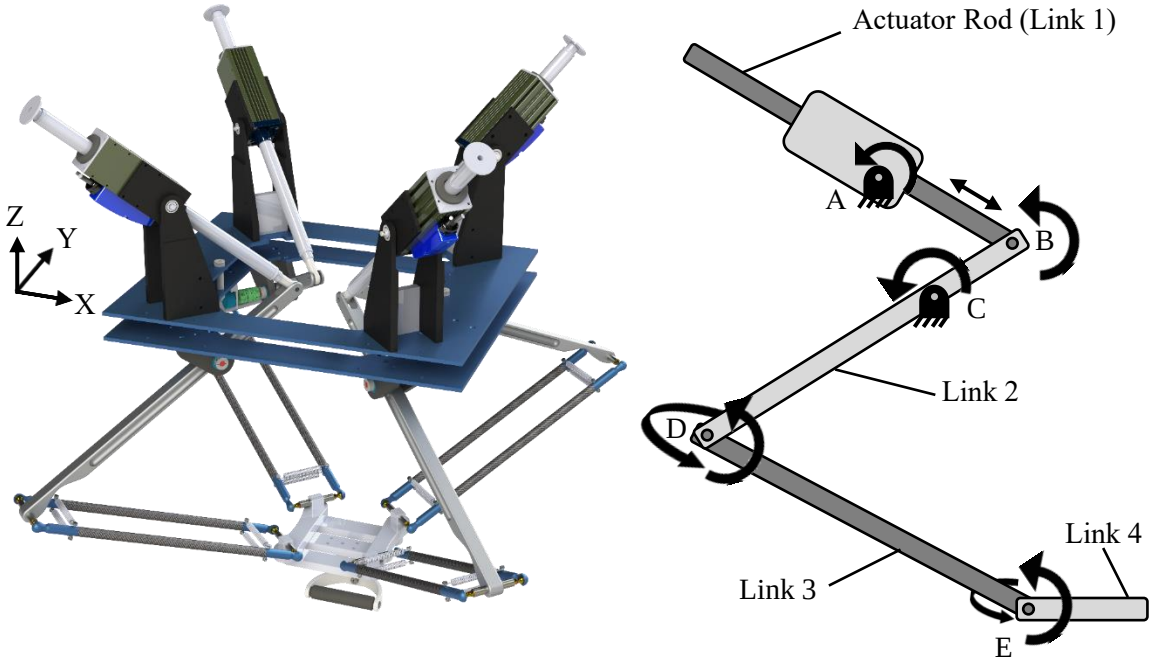

Figure 2.1. Details of the parallel arms of PARTNER. The left shows how the four identical arms are mounted onto two grounded mounting plates. The right highlights the three revolute, two universal, and one prismatic joints along a single parallel arm.

first chain. This closed chain is a type of slider-crank mechanism designed to control the angle of the Pivot Arm (Link 2).

The second part of a single parallel arm can be viewed as starting with Link 2 mounted at Point C. It is connected to Link 3 via a universal joint at Point D. Link 3, along with the same link from an adjacent parallel arm, then connects to a single side link of the end-effector (Link 4) at Point E via another universal joint. Finally the two side links (Link 4) of the end-effector are connected with the center piece via a revolute joint (not shown in Figure 2.1).

2.2 Structure

Two mechanical improvements were made to the structure of the robot. Section 2.2.1 discusses changes to the frame itself, while Section 2.2.2 discusses changes to the mounting plates.

2.2.1 Frame

In the early development of PARTNER, it was decided that the device should maintain as much portability as possible to accommodate transportation to other laboratories, both at the University of Idaho and externally. To achieve this design goal, the frame must not be rigidly attached to any part of the floor or wall of the room in which it is located. Additionally, the frame should be able to be taken apart, at least into moderate sized pieces, for transportation. Finally, the frame should be reconfigurable to allow for future design changes or improvements. After consideration of a few different materials, it was decided that the frame would be made from aluminum T-slot framing (produced by 80/20® Inc.).

An initial frame, shown on the left in Figure 2.2, was designed to accommodate the functional requirements of the robot, i.e. position the mechanism in the desired workplace and align different components of the mechanism relative to each other. It consists of various lengths of 1.5” T-slot extrusion, prefabricated angle braces, and aluminum joining brackets as

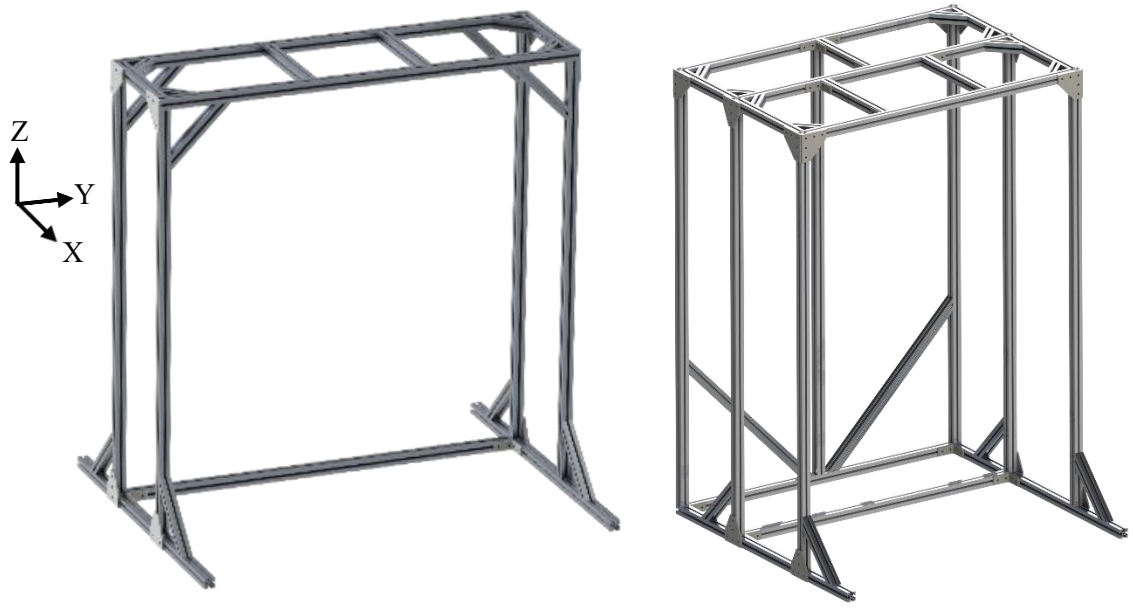

Figure 2.2 CAD showing the progression of the frame design. The first iteration is shown on the left, with a revised version on the right. The use of T-slot framing allowed for easy modification of the design to increase stiffness and accommodate other mechanical changes to the robot.

listed in Table 2.1. After some initial testing, it was quickly realized that the frame lacked proper rigidity due to the height of the structure and the lower than expected stiffness' of individual members. Specifically, a small torsional stiffness of the T-slot framing meant the two horizontal members on the floor were able to flex when the top platform was pushed side-to-side. This loading condition caused the top platform to translate on the order of two to three inches. Furthermore, the joints between adjacent 80/20 members using the 90° plates or T-plates, which rely on friction clamping to hold two members together, also introduced some unwanted flexibility of the frame.

To address this, a second iteration of the frame was developed. To address side-to-side flexibility of the frame, a third row of vertical supports was added with two 33" angle braces. The braces direct lateral forces into the frame's base and increase the overall stiffness. The third row also includes an additional vertical support beam to accommodate the hanging of a monitor on the frame. Additional 90° and "T" plates were added to joints to increase overall stiffness of the frame. The second iteration of the frame is not as rigid as desired, but the changes have made substantial improvements to the listed issues and brought the system to an acceptable level.

Table 2.1 Component quantities for the frame of PARTNER.

Component	Frame 1	Frame 2	McMaster #
Total Framing Length (m)	14.6	21.0	47065T102
6" Brace	4	8	47065T12
12" Brace	8	4	47065T27
33" Brace	0	2	-
90° Plate	4	8	47065T271
"T" Plate	4	7	47065T279

Future changes to the frame could address the remaining flexibility in a few ways. First, increasing the size of the 80/20 to 2” instead of 1.5” would increase individual member’s torsional stiffness dramatically. Because a future frame could build off of the general design of the existing system, the need for quick adjustment for potential design changes is less important. Thus a different style of framing material could be implemented such as steel or aluminum square tubing. If the current frame were kept, improvements could still be made by attaching it to the building, either by mounting it to a stud in the wall or a truss in the ceiling. This would be an easy solution, but would render the system less portable as any new location would require some preparations.

2.2.2 Mounting Plates

The mounting plates serve as a manner to connect the independent parallel arms to the common frame. Each arm must connect to the frame at two points, Points A and C in Figure 2.1, which must be properly aligned with respect to each other. The mounting plates also must properly align the four parallel arms with respect to each other. In the first prototype of PARTNER, it was thought that the 80/20 frame would properly align separate plates within an acceptable tolerance. As shown in Figure 2.3, the original design consisted of 8 small, separate mounting plates, to allow for simple manufacturing. Four were mounted above the frame for the actuator mounting (Upper Mounting Plates, shown in green) and four were located below the frame for the Pivot Arm mounts (Lower Mounting Plates, shown in yellow). After the first prototype was built, it was discovered that the plates were sufficiently misaligned to cause noticeable error in the end-effector location.

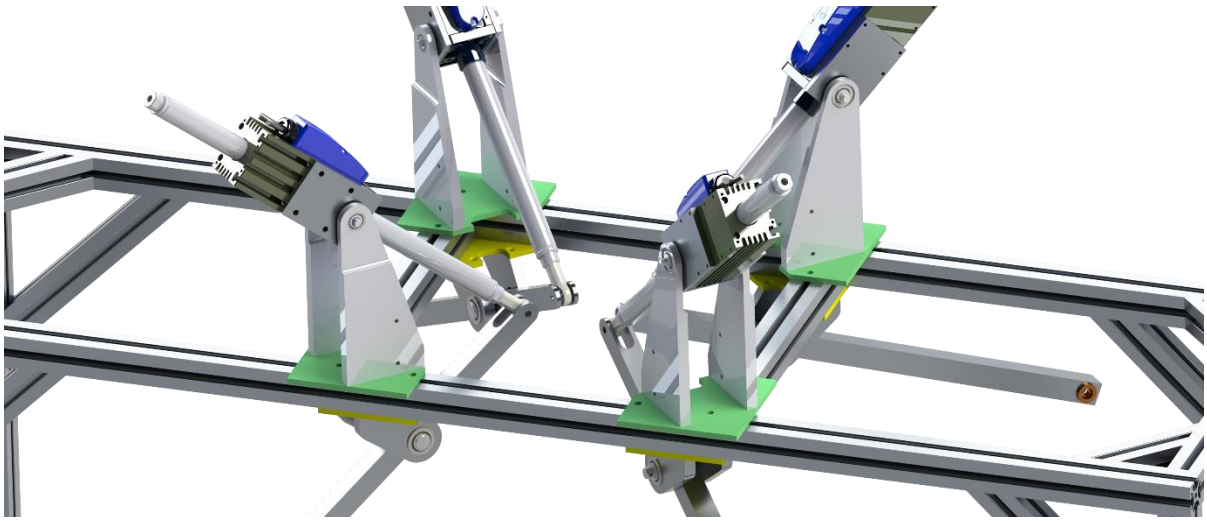

Figure 2.3 A rendering of the first iteration of mounting plates. The four green plates are identical Upper Mounting Plates. The four yellow plates are identical Lower Mounting Plates. While the independent plates were simple to manufacture, they proved inadequate at aligning the four parallel arms of the robot.

When measured, mounting plates were misaligned up to one cm. in both directions with respect to other plates on the same plane (Upper or Lower). The misalignment between upper and lower mounting plates was less severe. The misalignments were likely introduced into the system from tolerance stack-up issues during fabrication and assembly of the frame. The easily adjustable T-slot profiles, while allowing for quick adjustment and redesigns, proved to be an annoyance when precise alignment was desired. In an effort to avoid a complete remanufacture of all the mounting plates, an alignment jig was designed and laser cut to hold the plates relative to each other. However, after a few quick tests, it was decided that this solution would not properly address the problem and that a redesign of the plates was necessary.

The second iteration of the mounting plates reduces the number of separate plates from eight to two, one Upper Mounting Plate and one Lower Mounting Plate as seen in Figure 2.4. This ensures that the only misalignment introduced between components on the same plane (upper or lower) stem from errors in the manufacturing procedure. Due to the use of CNC equipment and careful machine shop practices, this error is now 0.08 mm, well within an

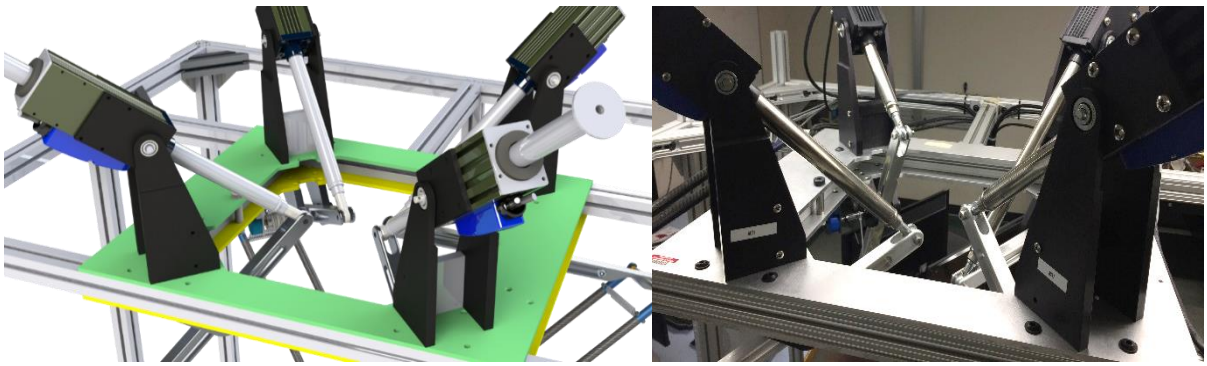

Figure 2.4 The second iteration of Mounting Plates. A shoulder bolt used for alignment of the upper and lower mounting plates can be seen on the left side of both images.

acceptable range. During assembly, the two plates are aligned using two ½ inch shoulder bolts before the frame is fully screwed together. This ensures that the frame conforms to the desired locations of the mounting plates, rather than plates conforming to the frame.

2.3 Pivot Bearing Assembly

The bearing assembly located at Point C in Figure 2.1 is crucial to the smooth operation of PARTNER. This is because the backlash from joints more distally located from the end-effector (i.e., Points A and B in Figure 2.1) is removed from the system at this point due to the grounding of Point C. In order to achieve the smoothest operation possible, significant attention was given to this assembly, prompting three iterations of the design. The first design consisted of two open, flanged bearings (Mcmaster-Carr Part No. 6383K234) press fit into grounded brackets and a steel flanged shaft (McMaster-Carr Part No. 97245A433) as shown in Figure 2.5. Between the two bearings, the shaft was passed through a reamed hole in link 2 and rigidly connected using a ¼-20 set screw. This ensured that the rotation of the link occurred at the bearing instead of between the shaft and Pivot Arm, while maintaining the ability to disassemble the system. The flanged end of the shaft only touched the inner race of the bearing, holding the shaft from slipping out of the right side. On the opposite end of the shaft, a cotter pin was placed through the shaft to keep it from sliding out to the left.

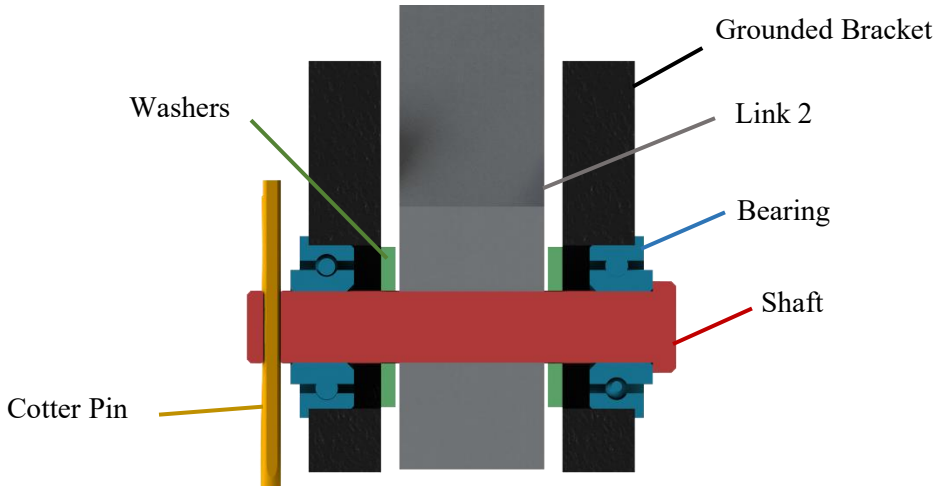

Figure 2.5 The first iteration of the pivot bearing assembly. The gap between the cotter pin and the left bearing introduced side-to-side backlash in Link 2.

The initial design had shortcomings that presented themselves after the first prototype was assembled, most notably the slop introduced to the system. The slop emerged from three primary flaws. First, the fit between the pivot shaft and the inner race of the bearings was too large. The intended design was a .0508 mm (0.002 in) slip fit. However, the actual fit was a .254 mm (.010 in) slip fit, derived from a 12.49 mm (0.492 in) shaft and 12.75 mm (0.502 in) bearing inner diameter. Second, the inner races of the bearings themselves had backlash that was unexpected. Finally, the pivot shaft was able to translate axially approximately 3.2 mm (1/8 in). The cotter pin kept the shaft from falling out of the assembly, but failed to keep the system sufficiently rigid. Using washers between Link 2 and the grounded brackets minimized this effect, but not without introducing unwanted friction to the system.

The second iteration addressed the identified issues from the first design. First, the purchased shaft was replaced with a custom machined shaft. The stock material was precision ground 12L14 steel, which ensures a properly sized diameter for the bearing fit. Second, a spring was added along the shaft's axis as can be seen in Figure 2.6. By turning the adjustment nut and compressing the spring, the spacer pushes against the inner race of the left bearing. The shaft collar on the right is then pulled against the inner race on the opposite bearing. This

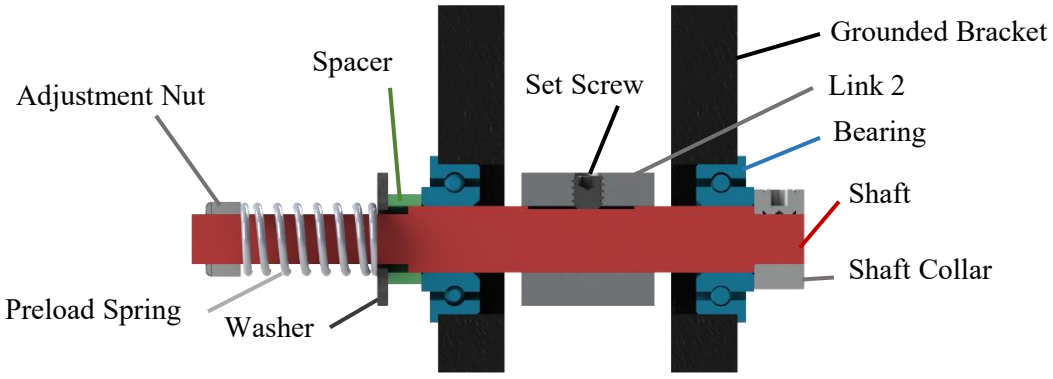

Figure 2.6 The second iteration of the pivot bearing assembly. A spring was added along the axis of the shaft to address slop from the bearings as well as to limit axial movement.

compression action preloads the inner races axially, which removes the extra unwanted movement. This adds a minimal amount of friction to the bearing. However, turning the adjustment nut allows balancing between the amount of introduced friction and amount of axial stiffness. Finally, flat surfaces were machined into the shaft to provide a better surface for the set screw to bite, without marring the surface unnecessarily.

The second iteration was a vast improvement over the first. The new shaft fit had a much tighter slip fit, with a 0.051 mm (0.002 in) clearance. The preload action drastically reduced the backlash in the system and the introduced friction was only noticeable at excessive preloads. The bearings, which were unchanged from the initial design, did prematurely wear however. This is likely due to excessive loads seen at the beginning of their life while in operation with the first iteration of the design. Additionally, a need arose for new shafts that could couple with potentiometers for redundant sensing (discussed further in Section 3.1). To address these issues, a third iteration of the system was designed.

The final iteration again built on the achievements made in the previous design and can be seen in Figure 2.7. The compression spring was replaced with a Belleville spring washer (McMaster-Carr Part No. 94065K54) to reduce the footprint while maintaining the functionality of the inner race preload. The bearings were replaced with double-shielded,

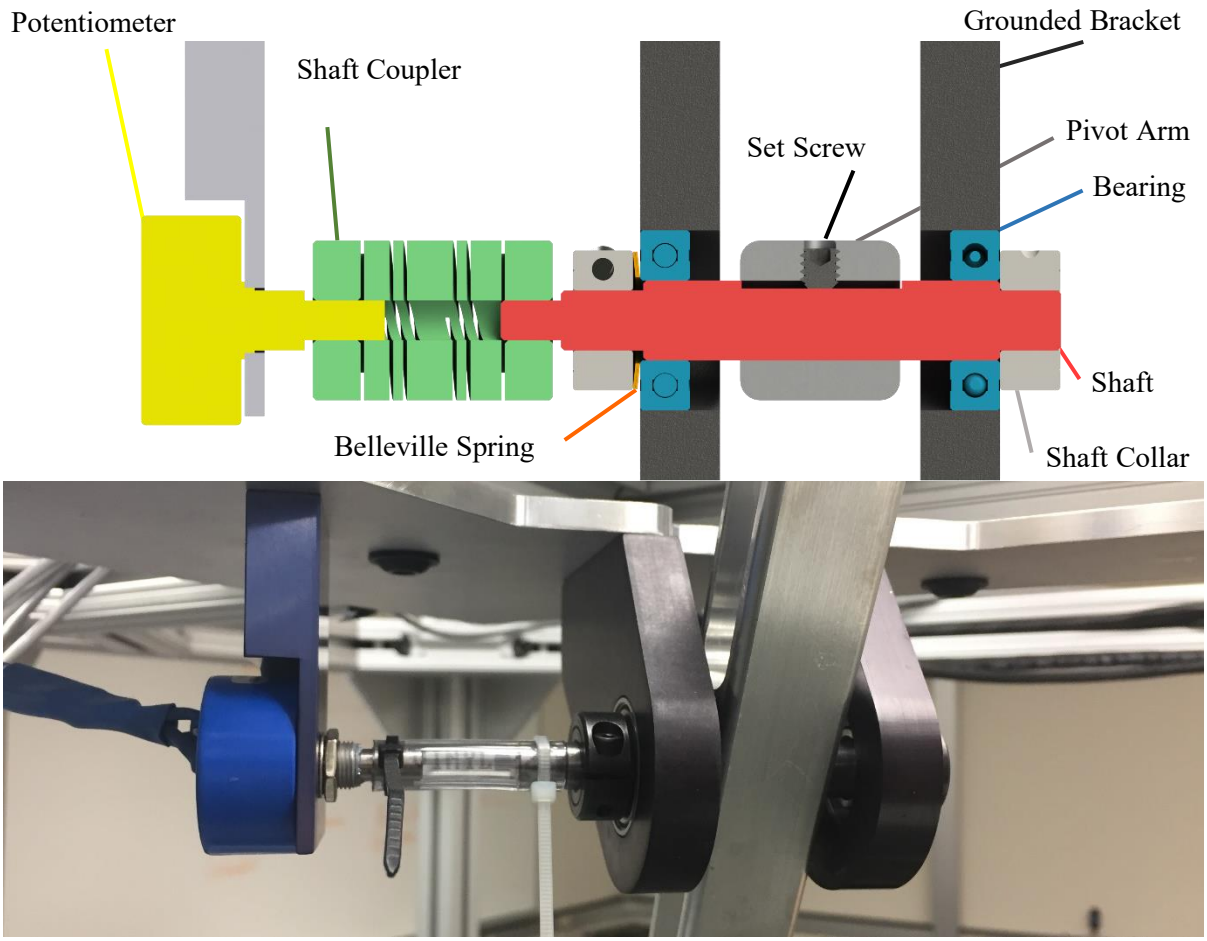

Figure 2.7 The third iteration of the pivot bearing assembly. The top shows the layout of the design, while the bottom is the installed version currently on PARTNER.

higher quality bearings (McMaster-Carr Part No. 60355K601). Finally, the end of the shaft was stepped down to allow a shaft coupling to connect the pivot shaft to a potentiometer.

These small changes improved the system substantially. The new bearings proved to be much tighter in tolerance, removing backlash and friction from the system. The Belleville style springs successfully preload the inner races of the bearings while only taking up a small portion of the assembly. The shaft coupling fits well and is easy to install and remove.

2.4 New Parallel Mechanism

The parallelogram link (Link 3) between Points D and E in Figure 2.1 must have a universal joint on both ends to create the desired mechanism. However, due to the large range of motion requirements (+/- 55° sideways, > 90° upwards), commercial off-the-shelf universal joints

(Figure 2.8, (a)) cannot be used. These requirements can be met by designing custom universal joints in which two revolute joints with intersecting axis are placed in series, but mechanically separated at a distance to provide the necessary clearance. In the first iteration of PARTNER, this double revolute style was implemented as shown in Figure 2.8 (b).

In the first design iteration, two bronze bushings (McMaster-Carr Part No. 1677K8) were pressed into the end of Link 2. A steel shaft was kept in place with two snap rings, located on the outside of either bronze bushing. At both ends of the shaft, clevis rod ends (Mcmaster-Carr Part No. 2449K14) are oriented orthogonally to the shaft and pinned through a reamed .953 cm (3/8 in) hole. Aluminum rods with threaded ends are screwed into the clevis rod ends, and the same joint design is replicated between Link 3 and the end-effector.

This first design was functional, but like the initial pivot bearing design, contained a lot of backlash. The plastic clevis rod ends gave too much flexibility. Depending on how much clearance was afforded with shims, the snap rings holding the shaft in place either permitted too much backlash or induced too much friction. The aluminum rods were screwed into the clevis rod ends, which would rotate when unexpected loading was placed on them. Even with Loctite applied to the connection, the joint would loosen over time. Finally, the long aluminum rods were not stiff enough, which caused them to deflect during use.

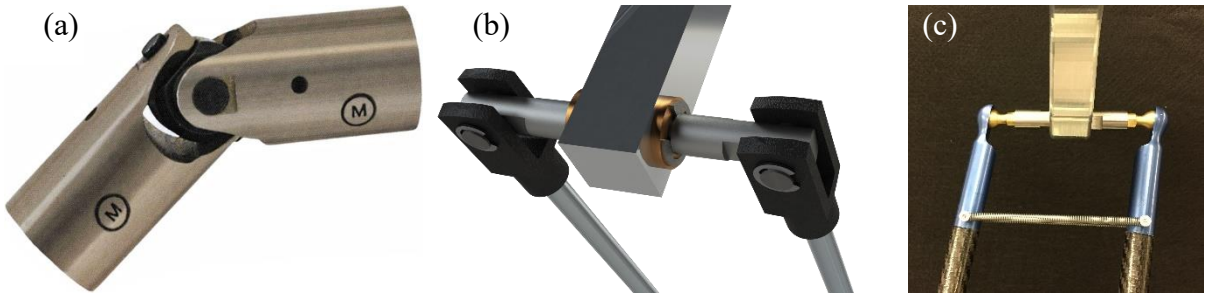

Figure 2.8 Different designs for a universal joint. (a) traditional cross style universal joint (b) 1st iteration of PARTNER joint design (c) 2nd iteration of PARTNER joint design.

To rectify these shortcomings, a second design using ball and cup joints was developed. Individually, each of the ball and cup joints would be a spherical joint with three DOFs, one more than the required two to complete a universal joint. The extra DOF is a rotation along the link's own axis. However practically, this extra DOF does not exist due to the dual tubes required to create the parallelogram shape for a single link. In the new design, the long aluminum rods are replaced with wrapped twill carbon fiber tubes (5/8" OD, ½" ID, Dragon Plate). This change of material and size increases the stiffness of the member by a factor of 14.6. Bonded to the ends of the carbon fiber are custom-machined aluminum end fittings. The bonding is achieved using 3M Scotch-Weld Epoxy EC-2216, with both surfaces prepared using the epoxy manufacturer's recommendations. This bonding method was tested on other projects at the University of Idaho and found to have a strength in this configuration in excess of 4000 N. In addition to machining the semi-sphere shape for the brass ball stud to fit in, small pockets of materials were removed at the base and lip of the cup to create wells for lubricant to reside, a common design feature in ball joints.

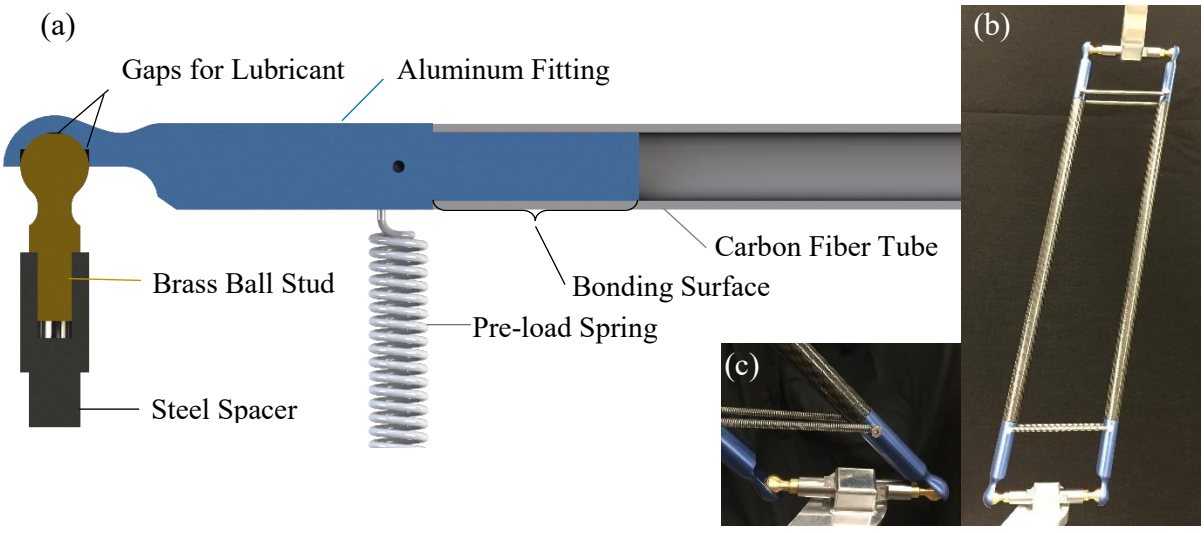

Figure 2.9 Design of Ball and Cup joint. (a) Section cut view of the details of a single ball and cup joint. (b) Picture of a complete Link 2 assembly (c) Picture of joint at end of ROM, -55° relative to vertical.

To hold the cup portions of the joint onto the ball studs, two springs are attached in parallel at each end of a single Link 2 assembly as shown in Figure 2.9 (b). The springs have a spring rate of 4.55 N/cm, initial pretension of 4.4 N and installed deflection of 2.54 cm (1 in) for a designed pre-load of 32 N (7.2 lbs) on each end. The springs are attached to the assembly by hooking onto shoulder bolts screwed into the aluminum fittings (Figure 2.9 (c)). The shoulder bolts keep the screws in place while allowing the hooks on the spring ends to rotate when the link is in movement. Two springs are used in place of a single, stiffer spring to curtail the extra DOF introduced with the spherical joint. Having a spring on either side of the rod balances the rotation along the rod's own axis.

2.5 New End Effector Rotation Mechanism

The final major mechanical design of the robot is the end effector rotation mechanism. This assembly requires three components: two identical side pieces (Link 4) and a center piece (Link 5) as shown below in Figure 2.10 (a). The two side pieces translate around the center of Link 5, while maintaining their orientation as shown in Figure 2.10 (b). Located on either end of Link 5 are revolute joints, shown as black dots that connect them to Link 4. On the outside ends of Link 4 are the universal joints (grey lines) that connect to Link 3 of the robot, shown

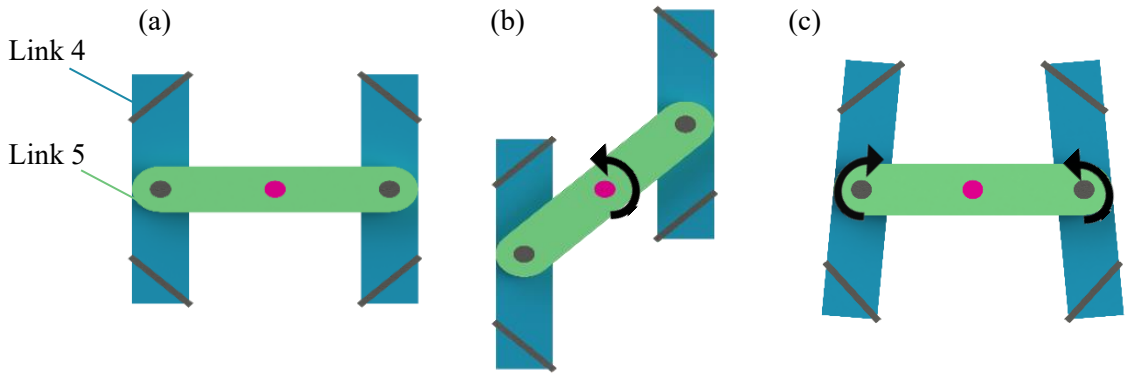

Figure 2.10 Different states of the end effector rotation mechanism. (a) The end effector rotation mechanism at θ = 0°. (b) The end effector rotation mechanism rotated to θ = 45° (c) Undesirable rotation of the side pieces in which the sides pinch together for an included angle of 5°.

as Point E in Figure 2.1. The universal joint style is as described in Section 2.4 , consisting of two ball and cup spherical joints.

The four arms of the robot theoretically force the two side pieces to stay parallel, thus only a single center piece should be necessary for the robot to function. In initial prototypes however, it was discovered that the two side pieces were able to pinch in at one end, with an included angle of approximately 5°. This is illustrated in Figure 2.10 (c). It was decided that removing this error by adding additional cross pieces would be the best course of action for the final design.

The final design consists of four pieces: two side links and two cross pieces. All four pieces are machined out of 6061-T6 aluminum on CNC equipment to ensure accurate spacing of joint locations. Significant material is removed from all four components to reduced weight, while strength is maintained via ribs as shown below in Figure 2.11 (a). The ball studs for the universal joint are screwed directly into angled extrusions on the side links. While these extrusions are a difficult manufacturing challenge, they ensure that all four sets of ball studs are correctly aligned.

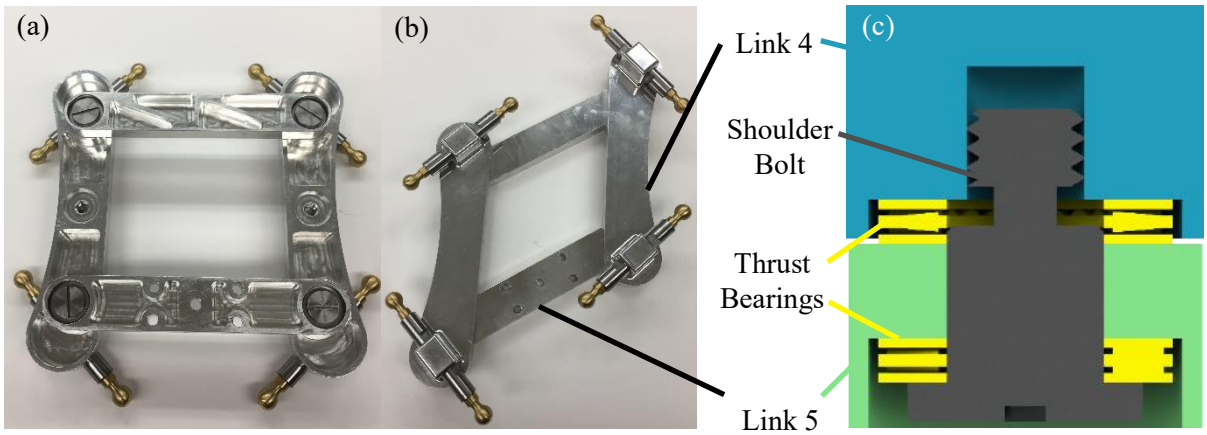

Figure 2.11 Details of the End Effector Rotation Mechanism. (a) Bottom view of the final design. (b) Top View of the final design. (c) Detailed cross-section of the joints.

The revolute joints (Figure 2.11 (c)) are designed to be as low profile as possible while limiting friction to a minimum. Thrust bearings are used in place of radial ball bearings as the loading is primarily axial along the joint. Custom shoulder bolts were machined out of 12L14 steel to make them as low profile as possible, as off the shelf shoulder bolts have large a head height ($^{5}/_{16}$" height for ½" shanks). The slip fit between the shoulder bolt and link 5 is 0.076 mm (0.003 in), which was found in testing to negate binding from misalignment across all the joints while not introducing slop in the system.

Chapter 3: Electronics and Control System Improvements

The four sections in this chapter present non-mechanical aspects of PARTNER. The first section describes different safety considerations taken in the development of the system. Section 3.2 describes two methods of localization. Next, the third section describes a model of the gravity effects on the robot. Finally, Section 3.4 presents and describes the frequency response of the robot, highlighting how the different axes exhibit similar dynamic behavior and system identification parameters.

3.1 Safety Considerations

In order to ensure a safe interaction between the user and the robot, a number of safeguards have been designed into PARTNER. The overall design of PARTNER is such that it provides a compliant interaction with the user, both with the power on and with the power off. The majority of the robot's structure self-balances itself, so in the event of a complete power-off, the user is not burdened with the vast majority of the robot's weight. In addition to the overall design of the robot, there are a few specific components included in the design targeted at safety, including multiple E-Stops and redundant position sensing.

Three emergency stop buttons are included on the robot: one next to the operator's computer and one on each side of the chair. The emergency stops (Mcmaster-Carr Part No. 6785K21) are all wired in a normally-closed design. This is to ensure that any change in the signal results in the robot's actuators turning off. Additionally, the emergency stop signal is run directly into the motor controller units, so any issues in the software or the data acquisition unit do not affect their function. Potential events that could bring about this change in signal include activation of any of the emergency stops, partial loss of power in the

system, disconnecting some or all of the data communication lines, or severing of the sensor lines.

Potentiometers (Bourns 6657S-1-103) are included on the pivots located at Point C in Figure 2.1 for use as a redundant position sensor. The potentiometers are coupled to the pivot shaft as shown in Figure 2.7. During use, the control system uses the potentiometer signals to calculate a redundant end-effector position and a discrepancy term,

$$D = \sqrt{\left(x_{diff}\right)^2 + \left(y_{diff}\right)^2 + \left(z_{diff}\right)^2 + .25\left(\theta_{diff}\right)^2}, \qquad \text{Eq. 1}$$

where D is the discrepancy, x_{diff}, y_{diff}, z_{diff}, and θ_{diff}, are the differences between the potentiometer and encoder based end-effector positions. The constant in front of the θ term is included to correct the scaling effects of different units (meters, radians). If the discrepancy, D, exceeds a pre-determined threshold, 0.05 m, then the robot stops operation.

3.2 Robot Localization

Position of the robot is obtained from the localization information obtained from the simulated incremental encoders embedded in the actuators (Dunkermoteren STA 2504). This measurement is very accurate, with a resolution of 12 microns, however it lacks an absolute position measurement. The result of this is a need to localize the robot upon startup. Two methods are available on the PARTNER robot.

The first method of initial localization is a slow homing procedure (about 8 seconds) in which the actuators are driven to a hard-stop and held while an incremental encoder measurement is taken. The actuator length at this point, $q_{max,}$ is constant and known a priori to be 0.4128 meters and the encoder measurement is saved as an offset, q_{offset}, to be used during operation. Two actuators are done simultaneously to save time. The actuator length is calculated during operation as

$$q_i = q_{measured,i} + q_{max} - q_{offset}, \quad \text{Eq. 2}$$

where q_i is the i[th] actuator location at a given moment, $q_{measured,i}$ is the i[th] encoder measurement at a given moment, and q_{max} and q_{offset} are as described above.

Because actuator locations are unknown during the homing procedure, position control cannot be used to drive the actuators to the hard stops. Instead, the forces seen in the actuator are ramped up from 0 to a max force of 36 Newtons, which ensures that the robot does not slam into the hard stops. An example of how the forces and measurements are taken during this procedure is shown below in Figure 3.1.

The second method for actuator localization uses the potentiometer described in Section 3.1 to find the offset. Upon start-up, the four potentiometers which are calibrated to Angle φ in Figure 3.2 and Figure 3.3 are measured. These angles are then converted to the actuator length

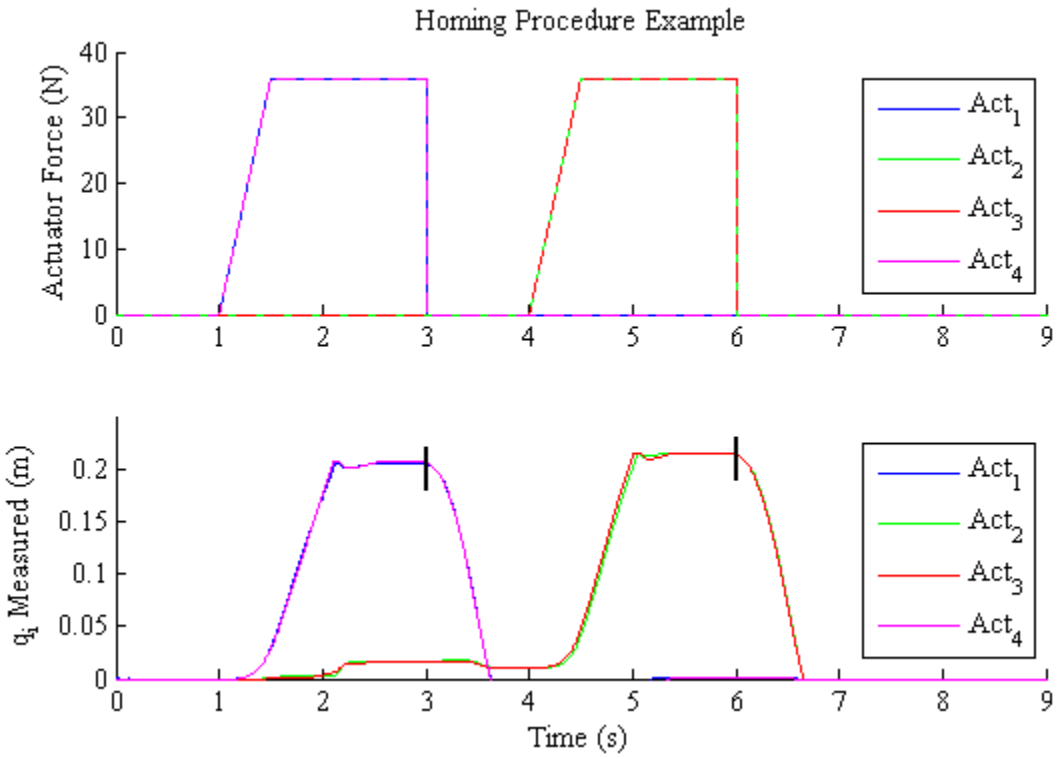

Figure 3.1 An example of the long localization procedure. The top graph shows the actuator forces during the procedure. The bottom graph shows the encoder measurements, $q_{measured,i}$, highlighting with a bolded vertical the times at which a reading is taken for the offset term in Equation 1.

using Equations 5 and 6 in the following section and saved as q_{offset} to be used in the same manner as the first method of localization. This localization method takes a fraction of a second and is not noticeable to the user.

Aside from differences in startup time, a few potential issues can dictate why one method should be used over the other. First, if the potentiometers slip within their shaft coupling, their calibration equation is no longer viable and the resultant offsets are incorrect. To address this concern, a mark has been applied across the shafts and coupling to track any slipping that occurs. Another concern is that a change in the supply voltage would also invalidate the calibration equation. To remedy this, the potentiometers are calibrated to normalized signal in which the potentiometer signal is divided by the voltage source. If for some reason the source signal is changed, the potentiometer signal would change at the same ratio, and the two changes would cancel each other out in the normalized variable.

3.3 Gravity Compensation

In order for PARTNER to balance itself at any location in the workspace, it is necessary to develop a model of the effects of gravity on the robot. While the mechanical design of PARTNER is such that most of robot weight self-balances with itself, it is not exact and varies across the workspace. This feed forward portion of the control system is designed to account for a static gravity balance of the robot, not including the effects of inertia or friction.

To begin, a free body diagram (Figure 3.2, left) of the pivot arm is drawn identifying the forces acting upon it. The actuator arm applies a force at Point B, along the axis of the actuator rod. Because of the revolute joint there, no moment is transferred from one member to another. There is a reaction force located at Point C from the lower pivot mount. The mass of the Pivot Arm can be applied as a point mass at the center of gravity of the member, W_{PA}. The steel and

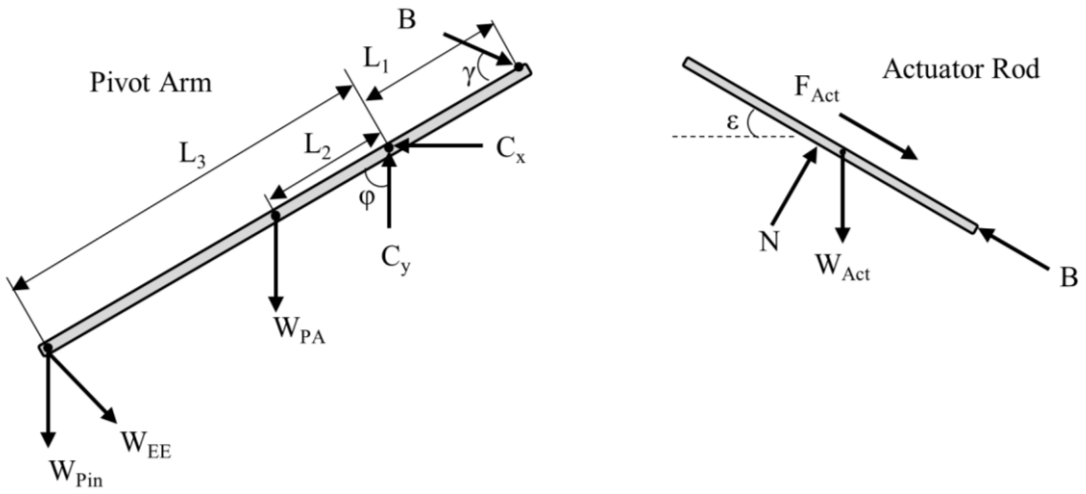

Figure 3.2 Free body diagram of the Pivot Arm and Actuator Rod.

brass inserts at the end of the pivot arm provide an additional load downward, W_{pin}. Finally, the parallelogram mechanism provides a force along its own axis, W_{EE}.

The weight of the parallelogram mechanism and the end-effector can be approximated as a point force at the location of the end-effector. Using the Jacobian (from [42]), this portion of the model will be accounted for at a later time. Summing the moments about Point C for the remaining forces, we find:

$$F_B = \frac{g \sin \varphi}{\sin \gamma}\left(m_{pa}L_2 + m_{pin}L_3\right), \qquad \text{Eq. 3}$$

where F_B is the interaction force between the actuator rod and the pivot arm, g is acceleration due to gravity, φ is the angle between the vertical and the pivot arm, γ is the angle between the Pivot Arm and the Actuator Rod, m_{pa} is the mass of the pivot arm, and m_{pin} is the mass of the pin.

Next we can look at the free body diagram for the Actuator Rod, shown on the right of Figure 3.2. Summing the forces along the axis of the rod we get:

$$F_{Act} = F_B - m_{Act} g \ \sin \varepsilon, \qquad \text{Eq. 4}$$

where F_{act} is the control force applied by the actuator, F_B is the interaction force between the Actuator Rod and the Pivot Arm, m_{Act} is the mass of the Actuator Rod, g is the acceleration due to gravity, and ε is the angle between the Actuator Rod and horizontal.

To determine the three angles (φ, γ, ε), the kinematic relationships of the arm must be developed. Figure 3.3 shows these relationships, highlighting the angles of the triangle defined by Points A, B, and C. Using the law of cosines, angles γ and β are found to be:

$$\gamma = \cos^{-1}\left(\frac{L_1^2 + q^2 - L_4^2}{2L_1 q}\right), \quad \text{Eq. 5}$$

$$\beta = \cos^{-1}\left(\frac{L_1^2 + L_4^2 - q^2}{2L_1 L_4}\right), \quad \text{Eq. 6}$$

where L_1 and L_4 are constant, known lengths, q is variable but known at all times from the robot's sensors. Angle φ can be found by examining Point C. Equating opposite angles,

$$\varphi = \beta - \theta, \quad \text{Eq. 7}$$

where θ is a known and constant angle. Angle ε can be found by looking at Point A. Summing the angles along the actuator rod we find:

$$\varepsilon = \gamma + \beta - \theta - \frac{\pi}{2}, \quad \text{Eq. 8}$$

where the variables are as defined in Figure 3.3.

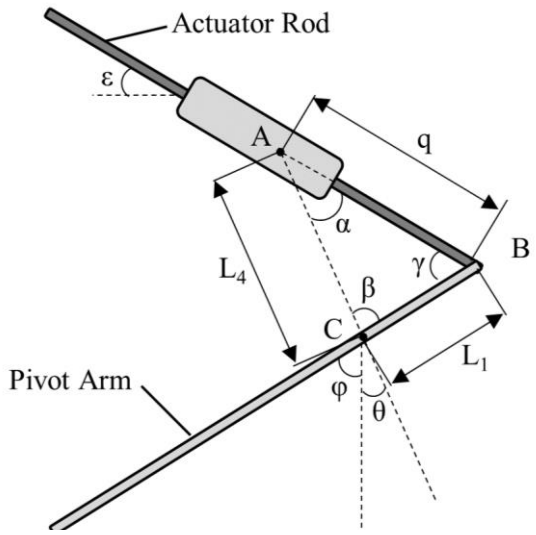

Figure 3.3 Kinematic diagram of one parallel arm.

Solving the system of equations above constitutes an approximation of the load from the Actuator Rod and the Pivot Arm. To complete the model, the effects of the parallelogram and end effector are approximated as a point force equal to their weight located at the end-effector and mapped to joint spaces using:

$$\boldsymbol{F}_{q,EE} = \boldsymbol{J}^T \boldsymbol{W}_{\boldsymbol{EE}}, \quad \text{Eq. 9}$$

where $\boldsymbol{F}_{q,EE}$ is the vector of the four actuator forces ($[F_1\ F_2\ F_3\ F_4]^T$) and $\boldsymbol{W}_{EE}$ is the vector of end-effector forces in x, y and z directions and the torque about z axis caused by the end effector ($[0\ 0\ W_{EE}\ 0]^T$). Summing the force from Equation 2 applied to each arm with the vector from Equation 7 completes the gravity compensation model.

3.4 Frequency Response Testing

Figure 3.4 shows the closed-loop frequency response of PARTNER for the three primary axes of translation. In separate experiments, the robot was excited by a sinusoidal desired trajectory with an amplitude of 0.02 m in each direction. The initial frequency was 1 Hz and increased by an increment of 0.05 Hz until a final frequency of 5 Hz. The control loop was closed with a proportional gain of 700 N/m and no integral or derivative terms.

Using this data, a second-order Mass-Spring-Damper dynamic model was fitted to each axis to characterize the robot. With a known feedback controller, the closed loop transfer function of the system is

$$G_{CL} = \frac{k_r K_c}{\frac{1}{\omega_n} s^2 + \frac{2\zeta}{\omega_n} s + k_r K_c + 1}, \quad \text{Eq. 10}$$

where k_r is the static gain of the system, K_c is the proportional controller gain (700 N/m), ω_n is the natural frequency of the robot in radians per second and ζ is the damping ratio. The closed-

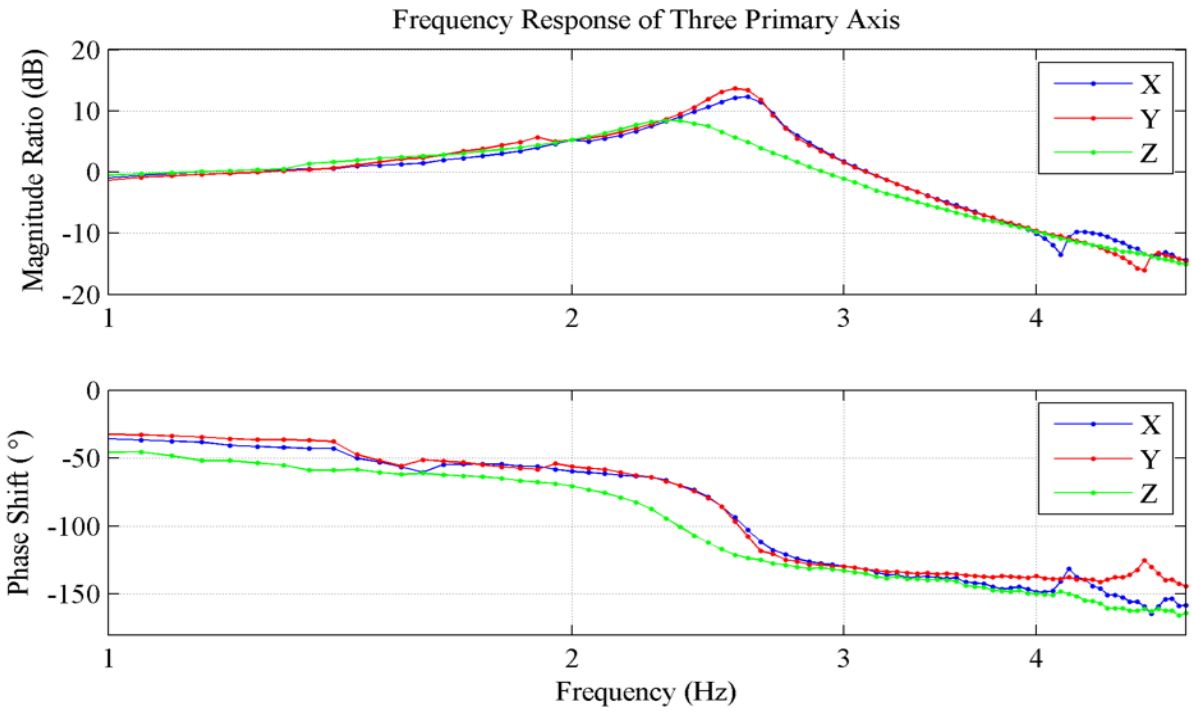

Figure 3.4 The frequency response of PARTNER. The blue, red, and green lines represent the X, Y, and Z directions respectively. Typical rehabilitation exercises are performed at frequencies well below the resonance band of the manipulator.

loop natural frequency of the whole system can be calculated from the system properties and controller parameters as

$$f_n = f_{n,robot}\sqrt{k_r K_c + 1}, \qquad \text{Eq. 11}$$

where f_n is the natural frequency of the closed-loop system in Hertz, $f_{n,robot}$ is ω_n converted from radians/second to Hertz, and the rest are as described for Equation 10. The three unknown parameters in model, k_r, ω_n, and ζ were fitted for each model using an optimization routine in which an error term comparing the experimental data and the model's magnitude ratio predictions was minimized. The experimental data and a fitted model for the X, Y, and Z axes can be seen below in Figures Figure 3.5, Figure 3.6, and Figure 3.7 respectively.

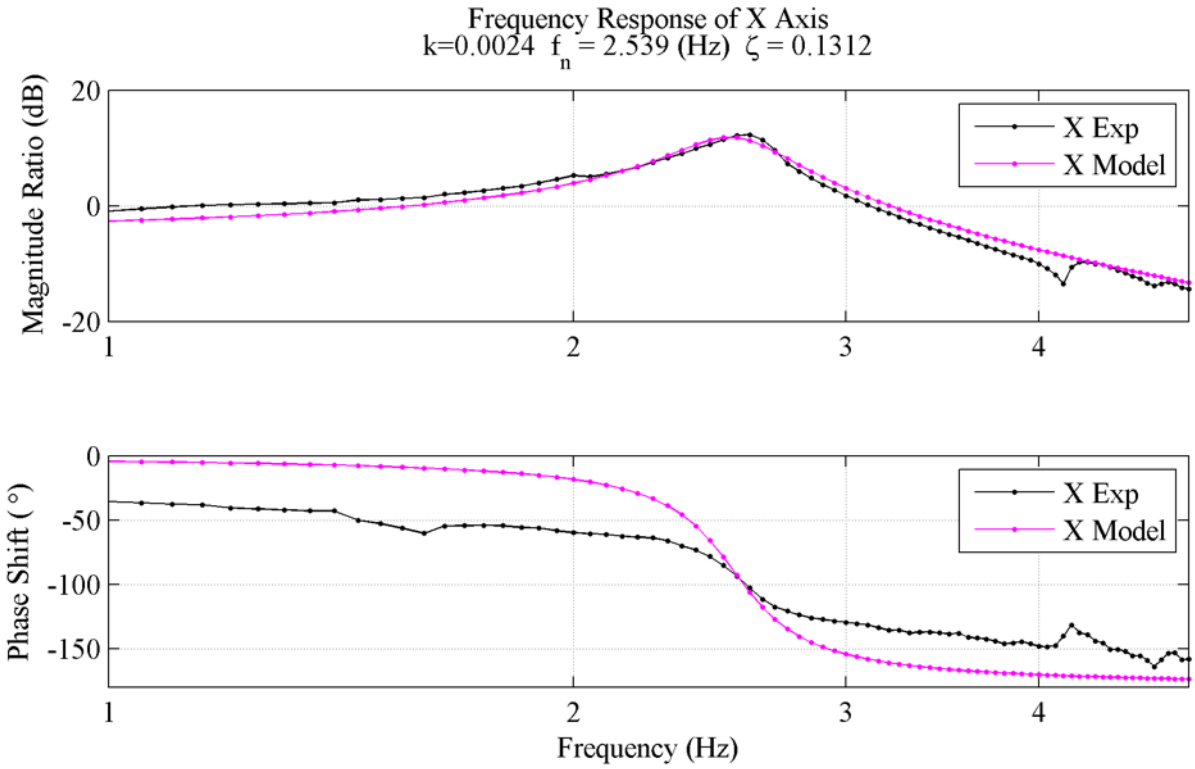

Figure 3.5 Frequency response and fitted model for the X axis.

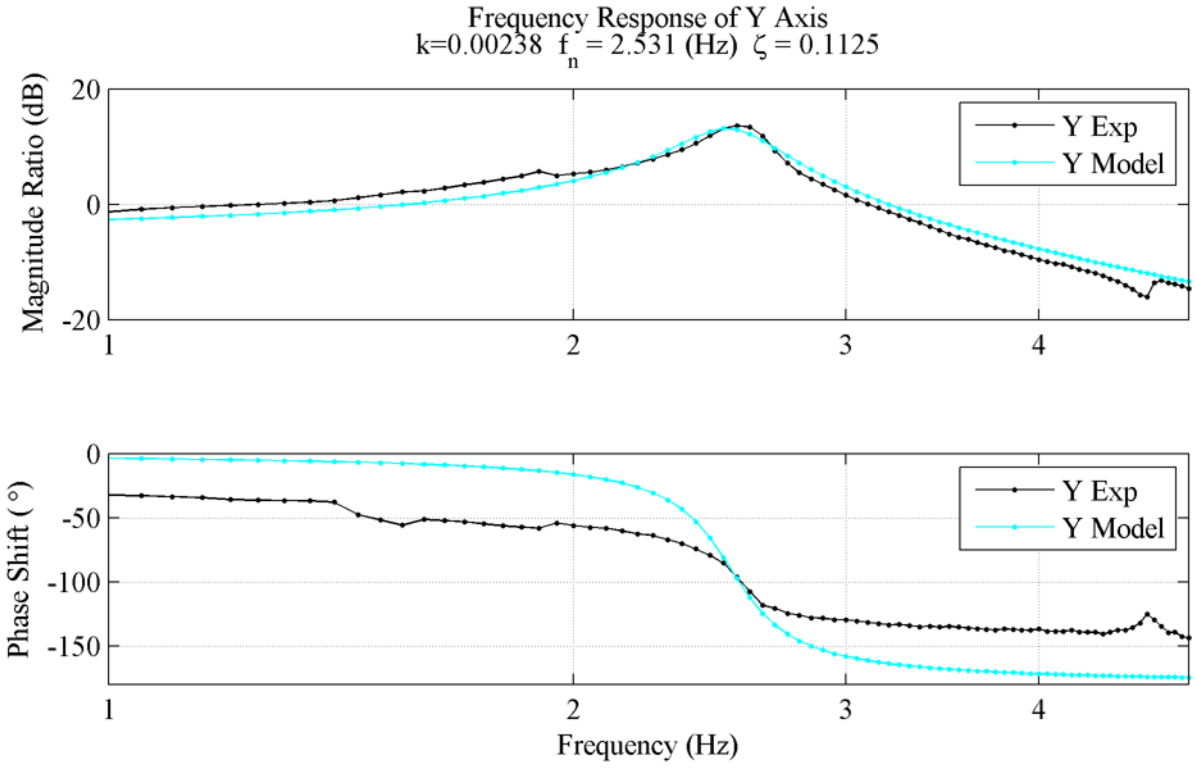

Figure 3.6 Frequency response and fitted model for the Y axis.

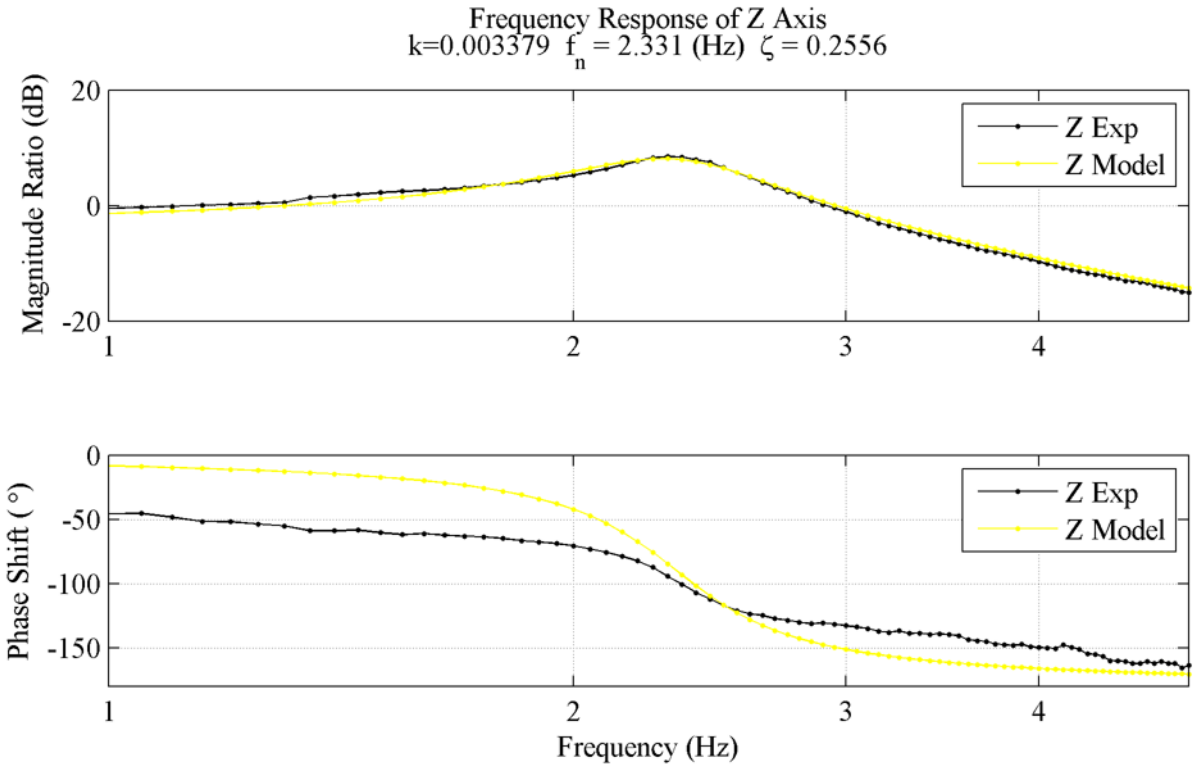

Figure 3.7 Frequency response and fitted model for the Z axis.

As it was stated in the introduction, a design goal of PARTNER was to have consistent performance across all three translational degrees of freedom. In the frequency response data, it can be see that that this goal was achieved. Of note however is the Z-axis beginning to attenuate slightly earlier than the X-axis and Y-axis, which are nearly identical. This is likely due to the kinematics of the robot and/or the effects of gravity on the robot that are more pronounced on this axis. The magnitude ratio stays above -3 dB until 3.33 Hz for both the X and Y axes, while the magnitude ratio for the Z axis cross -3 dB at 3.15 Hz.

Consistent performance can also be seen in the fitted model parameters, which are summarized below in Table 3.1. The X and Y axes have very similar system gain and natural frequency parameters, differing by 1.8% and 0.3% respectively. The damping ratio between these two axes is similar, but varies more than the other parameters at 15%. The Z axis model has similar behavior as the other two axes, but with a larger variation in specific parameter

values. Notably, the robot's natural frequency is 18% lower than the other two axes and the damping ratio is about double.

Table 3.1 Model Parameters

Model	System Gain, k_r	Robot Natural Freq, $f_{n,robot}$	Closed-loop Natural Freq, f_n	Damping Ratio, ζ
X Axis Model	0.002433	1.544 Hz	2.539 Hz	0.1328
Y Axis Model	.002389	1.548 Hz	2.531 Hz	.1125
Z Axis Model	.003378	1.271 Hz	2.331 Hz	.2556

The models were fit to the magnitude ratio data, not the phase shift data. In Figures Figure 3.5, Figure 3.6, and Figure 3.7, the phase shift experimental data follows the same pattern as the model. However, it is consistently larger before the corner frequency and smaller afterward. This trend is largely due to the un-modeled friction present in the system. At low frequencies, the robot stops before the apex of the desired trajectory. The static friction then holds it from moving back until the control commands enough force to break the static friction threshold. Because this phenomenon is un-modeled, it causes the larger than predicted delay. At higher frequencies, the robot has a smaller than predicted phase shift. Again, this is due to the same modeled friction present in the system. The friction helps reduce the momentum of the robot while changing directions, which causes the robot to take less time to change directions than predicted and reduces the phase shift.

Chapter 4: Results and Conclusions

This chapter presents a final conclusion of the work done on the PARTNER robot. The first section reviews my contributions to the project presented in the preceding chapters. The second section details suggestions for future work.

4.1 Summary of Work

The majority of my contributions to the project are the mechanical designs presented in Chapter 2. The designs for multiple iterations of the robot's structure, pivot bearing assemblies, and parallelogram linkage were described. On all these projects, I contributed to the first iteration in a minimal manner, but performed all tasks related to the design and fabrication of all subsequent iterations. I also contributed the entirety of the work presented in Section 2.5 pertaining to the end-effector rotation mechanism.

The structure of the robot was redesigned to stiffen the frame and correct alignment errors in the initial prototype. The aluminum extrusion frame was reconfigured with additional cross braces and vertical members to support the robot. The mounting plates that connect the frame to the rest of the robot were redesigned to be two individual plates instead of eight to correct the misalignment among the four parallel arms of PARTNER. These changes addressed the primary concerns and reduced the misalignment from 1 cm to 0.0762 mm.

The multiple iterations of the pivot bearing assembly were necessary to remove unwanted slop in the system and to integrate potentiometers to serve as redundant sensors. The final solution accomplished both of these requirements and leaves the robot moving in consistent, smooth manner.

The parallelogram linkage was changed from a long aluminum rod with a double revolute joint to carbon fiber tubes with ball and cup joints at the ends. These two design changes

significantly reduced flexion in the long rods as well as mechanical slop at the joints while maintaining a similar weight.

The final mechanical design contribution was the development of the end-effector rotation mechanism. The joint and linkage designs are mechanically simple, however much effort was put into manufacturing to ensure that the many critical dimensions were maintained. Specifically, the use of CNC equipment ensured that the holes for all the cross pieces were properly aligned to avoid binding in the system.

In addition to the contributions to mechanical designs, I also contributed to the electronics of PARTNER. I spearheaded the implementation of potentiometers at the pivot bearing location to serve as redundant position sensors and as a manner to localize the robot on start up. I also designed and implemented the emergency stop circuit, which disables the actuators at the user's discretion.

Finally, I contributed some basic control system necessities on PARTNER. Primarily, I developed two localization methods as presented in Section 3.2 and a gravity compensation model of the robot as presented in Section 3.3 . Both of these are currently implemented on PARTNER and work well. Additionally, I ran frequency response experiments on the robot and fit a 2^{nd} order dynamic model to each of the three primary axes, producing approximate system gain, natural frequency, and damping ratio values.

4.2 Suggestions for Future Work

PARTNER is currently a functioning robot and does not need many improvements or changes. One notable design challenge left to accomplish is the development of a sturdy handle that can securely attach to users. In the past, an undergraduate research team attempted to design and manufacture a handle, but the final product is severely lacking in functionality. It

does not strap the patient into the handle or provide any wrist support, thus requiring the patient to hold onto it the entire time. Before PARTNER is able to be used with any patients, this issue must be addressed.

A second issue to address with PARTNER is the development of interactive games. A simple reaching game was developed to showcase the robot for local high school students. The game consists of a randomly placed goal marker and a user-controlled robot marker showing where the robot currently is inside its workspace. The user must manipulate the robot's marker to the location of the robot marker, at which point the goal marker jumps to a new location and the user's score is increased by 1. The objective is to get as high of a score as possible in a given time period. While this game is functional, it severely lacks in visual appeal, motivation, and clear therapeutic goals. Adapting an existing therapeutic video game to work on the PARTNER system would be an excellent solution to this issue because of the possibilities of leveraging significant progress already made in the field of rehabilitation robotics.

Finally, with a model of the plant, work can begin on developing a compensator to manipulate the system dynamics as desired. Using the developed model, simulation software can be used to approximate controller parameters, which can then be quickly tested on the system, as all necessary mechanical and electrical requirements are complete.

References

[1] D. Mozaffarian *et al.*, "Heart Disease and Stroke Statistics—2016 Update: A Report From the American Heart Association," *Circulation,* December 16, 2015.

[2] V. L. Feigin *et al.*, "Global and regional burden of stroke during 1990–2010: findings from the Global Burden of Disease Study 2010," *The Lancet,* vol. 383, no. 9913, pp. 245-255, 2014.

[3] J. G. BROEKS, G. Lankhorst, K. Rumping, and A. Prevo, "The long-term outcome of arm function after stroke: results of a follow-up study," *Disability and rehabilitation,* vol. 21, no. 8, pp. 357-364, 1999.

[4] M. B. Buntin, C. H. Colla, P. Deb, N. Sood, and J. J. Escarce, "Medicare spending and outcomes after post-acute care for stroke and hip fracture," *Medical care,* vol. 48, no. 9, p. 776, 2010.

[5] D. X. Cifu and D. G. Stewart, "Factors affecting functional outcome after stroke: A critical review of rehabilitation interventions," *Archives of Physical Medicine and Rehabilitation,* vol. 80, no. 5, pp. S35-S39, May 1999.

[6] D. U. Jette, N. K. Latham, R. J. Smout, J. Gassaway, M. D. Slavin, and S. D. Horn, "Physical therapy interventions for patients with stroke in inpatient rehabilitation facilities," *Physical therapy,* vol. 85, no. 3, pp. 238-248, 2005.

[7] P. Duncan, "Synthesis of intervention trials to improve motor recovery following stroke," *Topics in Stroke Rehabilitation,* vol. 3, no. 4, pp. 1-20, 1997.

[8] L. Richards and P. Pohl, "Therapeutic interventions to improve upper extremity recovery and function," *Clinics in geriatric medicine,* vol. 15, no. 4, pp. 819-832, 1999.

[9] J. H. van der Lee, I. A. Snels, H. Beckerman, G. J. Lankhorst, R. C. Wagenaar, and L. M. Bouter, "Exercise therapy for arm function in stroke patients: a systematic review of randomized controlled trials," *Clinical Rehabilitation,* vol. 15, no. 1, pp. 20-31, 2001.

[10] K. R. Lohse, C. E. Lang, and L. A. Boyd, "Is more better? Using metadata to explore dose–response relationships in stroke rehabilitation," *Stroke,* vol. 45, no. 7, pp. 2053-2058, 2014.

[11] R. W. Teasell, N. C. Foley, S. K. Bhogal, and M. R. Speechley, "An evidence-based review of stroke rehabilitation," *Topics in stroke Rehabilitation,* 2015.

[12] H.-C. Huang, K.-C. Chung, D.-C. Lai, and S.-F. Sung, "The impact of timing and dose of rehabilitation delivery on functional recovery of stroke patients," *Journal of the Chinese Medical Association,* vol. 72, no. 5, pp. 257-264, 2009.

[13] M. Lotze, C. Braun, N. Birbaumer, S. Anders, and L. G. Cohen, "Motor learning elicited by voluntary drive," *Brain,* vol. 126, no. 4, pp. 866-872, 2003.

[14] N. Hogan, H. I. Krebs, B. Rohrer, and J. J. Palazzolo, "Motions or muscles? Some behavioral factors underlying robotic assistance of motor recovery," *Journal of rehabilitation research and development,* vol. 43, no. 5, p. 605, 2006.

[15] N. C. Bejarano, S. Maggioni, L. De Rijcke, C. A. Cifuentes, and D. J. Reinkensmeyer, "Robot-Assisted Rehabilitation Therapy: Recovery Mechanisms and Their Implications for Machine Design," in *Emerging Therapies in Neurorehabilitation II*: Springer, pp. 197-223, 2016.

[16] M. Rensink, M. Schuurmans, E. Lindeman, and T. Hafsteinsdottir, "Task-oriented training in rehabilitation after stroke: systematic review," *Journal of advanced nursing,* vol. 65, no. 4, pp. 737-754, 2009.

[17] A. A. Timmermans, A. I. Spooren, H. Kingma, and H. A. Seelen, "Influence of Task-Oriented Training Content on Skilled Arm–Hand Performance in Stroke: A Systematic Review," *Neurorehabilitation and neural repair,* vol.24, no. 9, pp. 858-870, 2010.

[18] D. J. Reinkensmeyer and M. L. Boninger, "Technologies and combination therapies for enhancing movement training for people with a disability," *Journal of neuroengingeering and rehabilitation,* vol. 9, p. 17, 2012.

[19] R. Colombo *et al.*, "Design strategies to improve patient motivation during robot-aided rehabilitation," *Journal of neuroengineering and rehabilitation,* vol. 4, no. 1, p. 1, 2007.

[20] D. J. Reinkensmeyer, J. L. Emken, and S. C. Cramer, "Robotics, motor learning, and neurologic recovery," *Annual review of biomedeical engineering,* vol. 6, pp. 497-525, 2004.

[21] N. Norouzi-Gheidari, P. S. Archambault, and J. Fung, "Effects of robot-assisted therapy on stroke rehabilitation in upper limbs: systematic review and meta-analysis of the literature," *Journal of rehabilitation research and development,* vol. 49, no. 4, pp. 479-496, 2012.

[22] G. B. Prange, M. J. Jannink, C. G. Groothuis-Oudshoorn, H. J. Hermens, and M. J. IJzerman, "Systematic review of the effect of robot-aided therapy on recovery of the hemiparetic arm after stroke," *Journal of rehabilitation research and development,* vol. 43, no. 2, p. 171, 2006.

[23] G. Kwakkel, B. J. Kollen, and H. I. Krebs, "Effects of robot-assisted therapy on upper limb recovery after stroke: a systematic review," *Neurorehabilitation and neural repair,* 2007.

[24] P. Sale, M. Franceschini, S. Mazzoleni, E. Palma, M. Agosti, and F. Posteraro, "Effects of upper limb robot-assisted therapy on motor recovery in subacute stroke patients," *Journal of neuroengineering and rehabilitation,* vol. 11, no. 1, p. 1, 2014.

[25] J. Mehrholz, A. Hädrich, T. Platz, J. Kugler, and M. Pohl, "Electromechanical and robot-assisted arm training for improving generic activities of daily living, arm function, and arm muscle strength after stroke," *The Cochrane Library,* 2012.

[26] J. C. Perry, J. Rosen, and S. Burns, "Upper-limb powered exoskeleton design," *IEEE/ASME transactions on mechatronics,* vol. 12, no. 4, p. 408, 2007.

[27] B. Kim and A. D. Deshpande, "Controls for the shoulder mechanism of an upper-body exoskeleton for promoting scapulohumeral rhythm," *IEEE International Conference on Rehabilitation Robotics (ICORR) 2015*, pp. 538-542, 2015.

[28] M. Mihelj, T. Nef, and R. Riener, "ARMin-toward a six DoF upper limb rehabilitation robot," *The First IEEE/RAS-EMBS International Conference on Biomedical Robotics and Biomechatronics (BioRob), 2006.*, pp. 1154-1159, 2006.

[29] L. Marchal-Crespo and D. J. Reinkensmeyer, "Review of control strategies for robotic movement training after neurologic injury," *Journal of neuroengineering and rehabilitation,* vol. 6, no. 1, p. 20, 2009.

[30] H. I. Krebs, N. Hogan, M. L. Aisen, and B. T. Volpe, "Robot-aided neurorehabilitation," *IEEE transactions on rehabilitation engineering,* vol. 6, no. 1, pp. 75-87, 1998.

[31] Bionik. (9/26/2016). *Upper Extremity Rehabilitation*. Available: http://bionikusa.com/healthcarereform/upper-extremity-rehabilitiation/

[32] H. I. Krebs *et al.*, "Rehabilitation robotics: pilot trial of a spatial extension for MIT-Manus," *Journal of NeuroEngineering and Rehabilitation,* vol. 1, no. 1, p. 5, 2004.

[33] M. Schoone, P. Van Os, and A. Campagne, "Robot-mediated Active Rehabilitation (ACRE) A user trial," *IEEE 10th International Conference on Rehabilitation Robotics, (ICORR 2007)*, pp. 477-481, 2007.

[34] G. Rosati, P. Gallina, S. Masiero, and A. Rossi, "Design of a new 5 dof wire-based robot for rehabilitation," *IEEE 9th International Conference on Rehabilitation Robotics (ICORR 2005),* pp. 430-433, 2005.

[35] R. Riener, T. Nef, and G. Colombo, "Robot-aided neurorehabilitation of the upper extremities," *Medical and Biological Engineering and Computing,* vol. 43, no. 1, pp. 2-10, 2005.

[36] R. C. Loureiro, W. S. Harwin, K. Nagai, and M. Johnson, "Advances in upper limb stroke rehabilitation: a technology push," *Medical & biological engineering & computing,* vol. 49, no. 10, pp. 1103-1118, 2011.

[37] P. Maciejasz, J. Eschweiler, K. Gerlach-Hahn, A. Jansen-Troy, and S. Leonhardt, "A survey on robotic devices for upper limb rehabilitation," *J. Neuroeng. Rehabil,* vol. 11, no. 3, p. 10.1186, 2014.

[38] L. Cai *et al.*, "Effects of consistency vs. variability in robotically controlled training of stepping in adult spinal mice," in *IEEE 9th International Conference on Rehabilitation Robotics (ICORR 2005)*, pp. 575-579, 2005.

[39] R. A. Schmidt and T. Lee, *Motor control and learning*. Human kinetics, 1988.

[40] S. Masiero, E. Carraro, C. Ferraro, P. Gallina, A. Rossi, and G. Rosati, "Upper limb rehabilitation robotics after stroke: a perspective from the University of Padua, Italy," *Journal of Rehabilitation Medicine,* vol. 41, no. 12, pp. 981-985, 2009.

[41] F. Pierrot, F. Marquet, O. Company, and T. Gil, "H4 parallel robot: modeling, design and preliminary experiments," *IEEE International Conference on Robotics and Automation (ICRA 2001)*, vol. 4, pp. 3256-3261, 2004.

[42] H. Taheri, "Robotic Devices and Adaptive Control Strategies for Robotic Rehabilitation After Stroke," Ph.D, Department of Mechanical Engineering, University of Idaho, 932368749, 2014.

[43] H. Taheri, S. A. Goodwin, J. A. Tigue, J. C. Perry, and E. T. Wolbrecht, "Design and Optimization of PARTNER: a Parallel Actuated Robotic Trainer for NEuroRehabilitation," *38th Annual International Conference of the Engineering in Medicine and Biology Society (EMBC 16),* pp. 2128-2132, 2016.

k